

# CSF1R inhibition delays cervical and mammary tumor growth in murine models by attenuating the turnover of tumor-associated macrophages and enhancing infiltration by CD8<sup>+</sup> T cells

Debbie C Strachan<sup>1,†</sup>, Brian Ruffell<sup>2</sup>, Yoko Oei<sup>1</sup>, Mina J Bissell<sup>3</sup>, Lisa M Coussens<sup>2</sup>, Nancy Pryer<sup>1</sup>, and Dylan Daniel<sup>1,\*</sup>

<sup>1</sup>Novartis Institutes for Biomedical Research; Emeryville, CA USA; <sup>2</sup>Department of Cell and Developmental Biology and Knight Cancer Institute; Oregon Health and Science University; Portland, OR USA; <sup>3</sup>Life Sciences Division, Lawrence Berkeley National Laboratory, Berkeley, CA USA

<sup>†</sup>Current address: Cellera Therapeutics; San Carlos, CA USA

**Keywords:** breast cancer, cervical cancer, CSF1R, M-CSF, tumor-associated macrophages, tumor immune evasion, tumor immunology, transgenic mouse models

**Abbreviations:** CSF1, colony stimulating factor 1; *Csf1<sup>op</sup>*, *Csf1*-nullizygous mouse; CSF1R, CSF1 receptor; EGF, epidermal growth factor; HPV-16, human papilloma virus type 16; IL, interleukin; K14, keratin 14; MMTV, mouse mammary tumor virus; PyMT, polyomavirus middle T antigen; TAM, tumor-associated macrophage

Increased numbers of tumor-infiltrating macrophages correlate with poor disease outcome in patients affected by several types of cancer, including breast and prostate carcinomas. The colony stimulating factor 1 receptor (CSF1R) signaling pathway drives the recruitment of tumor-associated macrophages (TAMs) to the neoplastic microenvironment and promotes the differentiation of TAMs toward a pro-tumorigenic phenotype. Twelve clinical trials are currently evaluating agents that target the CSF1/CSF1R signaling pathway as a treatment against multiple malignancies, including breast carcinoma, leukemia, and glioblastoma. The blockade of CSF1R signaling has been shown to greatly decrease the number of macrophages in a tissue-specific manner. However, additional mechanistic insights are needed in order to understand how macrophages are depleted and the global effects of CSF1R inhibition on other tumor-infiltrating immune cells. Using BLZ945, a highly selective small molecule inhibitor of CSF1R, we show that CSF1R inhibition attenuates the turnover rate of TAMs while increasing the number of CD8<sup>+</sup> T cells that infiltrate cervical and breast carcinomas. Specifically, we find that BLZ945 decreased the growth of malignant cells in the mouse mammary tumor virus-driven polyomavirus middle T antigen (MMTV-PyMT) model of mammary carcinogenesis. Furthermore, we show that BLZ945 prevents tumor progression in the keratin 14-expressing human papillomavirus type 16 (K14-HPV-16) transgenic model of cervical carcinogenesis. Our results demonstrate that TAMs undergo a constant turnover in a CSF1R-dependent manner, and suggest that continuous inhibition of the CSF1R pathway may be essential to maintain efficacious macrophage depletion as an anticancer therapy.

## Introduction

Tumor-associated macrophages (TAMs) represent the most abundant cells of the immune system found within the stroma of some malignancies,<sup>1-3</sup> and increased TAM density has been correlated with poor prognosis in patients affected by several cancers including breast, prostate, ovarian, and cervical carcinomas.<sup>4</sup> Conversely, in a smaller subset of malignant diseases, including gastric and lung cancer, the presence of TAMs actually correlates with a favorable outcome,<sup>4</sup> a discrepancy that can potentially be ascribed to functionally distinct and tissue-specific subtypes of

macrophages. The widely used M1-M2 macrophage classification scheme highlights an apparent range of macrophage functions.<sup>5</sup> M1, “classically activated” macrophages secrete pro-inflammatory cytokines as part of T<sub>H</sub>1 immune responses and can be tumoricidal in vitro.<sup>6</sup> In contrast, M2, “alternatively activated” macrophages respond to T<sub>H</sub>2 cytokines involved in tissue repair and wound healing, and as such can play an immunosuppressive role.<sup>7</sup> TAMs, however, are unique in that they can exhibit both M1- and M2-type properties, suggesting the existence of hybrid macrophage phenotypes<sup>8,9</sup> that fit into a classification scheme

\*Correspondence to: Dylan Daniel; Email: dylan.daniel@novartis.com

Submitted: 09/24/2013; Revised: 10/24/2013; Accepted: 10/26/2013; Published Online: 12/04/2013

Citation: Strachan DC, Ruffell B, Oei Y, Bissell M, Coussens LM, Pryer N, Daniel D. CSF1R inhibition delays cervical and mammary tumor growth in murine models by attenuating the turnover of tumor-associated macrophages and enhancing infiltration by CD8<sup>+</sup> T cells. *Oncoimmunology* 2013; 2:e26968; <http://dx.doi.org/10.4161/onci.26968>

in which macrophage subtypes span a continuous spectrum of overlapping features.<sup>10</sup> This said, breast cancer-associated macrophages often display an M2 phenotype<sup>5,11</sup> and promote tumor invasion and metastasis *in vivo*.<sup>12,13</sup>

The signaling axis mediated by colony-stimulating factor 1 (CSF1) and its cognate receptor CSF1R has been widely characterized as a key regulator of monocyte differentiation as well as of the generation and activity of tissue-resident macrophages.<sup>3,14,15</sup> *Csf1<sup>op</sup>* mice, which are nullizygous for CSF1, lack osteoclasts and are consequently osteopetrotic, although these animals display an incomplete loss of tissue macrophages.<sup>16</sup> In comparison, *Csf1r<sup>-/-</sup>* mice display a phenotype that partially overlaps with that of *Csf1<sup>op</sup>* mice, as for instance the former also manifest a loss of Langerhans cells.<sup>17</sup> The increased severity of the phenotype of *Csf1r<sup>-/-</sup>* mice can be explained by the disrupted signaling of another, CSF1-independent CSFR1 ligand, interleukin (IL)-34.<sup>18,19</sup> Although IL-34 has been found to bind CSF1R with higher affinity than CSF1, and can substitute for CSF1 in myeloid cell development *in vitro*,<sup>18</sup> pronounced differences in tissue expression indicate that IL-34 is more likely to have a predominant role in CSF1R signaling in the brain as compared with other tissues.<sup>19</sup>

The overexpression of CSF1 is associated with poor prognosis in subjects with breast, ovarian, and prostate cancer,<sup>1,20</sup> and a CSF1-responsive signature has been shown to prognosticate disease recurrence and invasiveness,<sup>21</sup> as well as tumor grade, in (at least some subsets of) breast cancer patients.<sup>22</sup> In overlapping indications, this reflects the aforementioned clinical data ascribing increased TAM density with a poor prognostic value, suggesting that CSF1/CSF1R may play a critical and preferential role in driving the activity of tumor-promoting macrophages.

In support of this notion, *Csf1<sup>op</sup>* mice crossed into the mouse mammary tumor virus- polyomavirus middle T antigen (MMTV-PyMT) transgenic model of mammary carcinogenesis display a striking reduction in pulmonary metastasis, despite the fact that there is no apparent difference in the incidence or growth of multi-focal, primary mammary tumors.<sup>23</sup> Conversely, pharmacological inhibition of CSF1R in MMTV-PyMT transgenic mice has been previously reported to affect tumor growth by enhancing chemotherapeutic responses in a CD8<sup>+</sup> T cell-dependent manner.<sup>24</sup> In combination with prior work demonstrating the role of CD4<sup>+</sup> T cells in promoting the pro-tumorigenic activities of TAMs in MMTV-PyMT mice,<sup>11</sup> these studies raise the question of how the CSF1R pathway mechanistically regulates the abundance and activity TAMs, and indicate a link between CSF1R-driven TAMs and tumor-infiltrating T cells in the maintenance of an immunosuppressive tumor microenvironment.

Here, we employed MMTV-PyMT transgenic mice to identify a specific population of TAMs, an approach revealing that CSF1R stimulation is essential to maintain the rapid turnover rate of TAMs *in vivo*. Using a highly selective CSF1R inhibitor, BLZ945, we found that TAMs typically recirculate in and out of neoplastic lesions within 5 d. Furthermore, we also found that CSF1R inhibition markedly decreases the recruitment of macrophages to the malignant site and enhances tumor-infiltration by CD8<sup>+</sup> T cells. Upon the administration of BLZ945, CSF1R-dependent, immunological alterations of the

tumor microenvironment limited mammary tumor growth in mice orthotopically allografted with cancer cells derived from MMTV-PyMT transgenic animals. Similarly, using the keratin 14-expressing human papillomavirus type 16 (K14-HPV-16) transgenic model of cervical carcinogenesis,<sup>25</sup> we also demonstrated that the pharmacologic inhibition of CSF1R decreases the abundance of macrophages within cervical tumors and the associated stroma, an effect that suffices to inhibit the growth of established neoplasms.

## Results

### Mammary tumors from MMTV-PyMT transgenic mice contain macrophages with a regulatory phenotype

Spontaneous mammary tumors from 63- to 77 d old female MMTV-PyMT transgenic mice were dissociated into single-cell suspensions and analyzed by multicolor flow cytometry. TAMs were identified as CD45<sup>+</sup>CD11b<sup>+</sup>Ly6G<sup>-</sup>Ly6C<sup>lo</sup>F4/80<sup>+</sup> cells (Fig. 1A). In order to characterize the differentiation state of the TAMs, CD45<sup>+</sup>CD11b<sup>+</sup>Ly6G<sup>-</sup>Ly6C<sup>lo</sup>F4/80<sup>+</sup> cells were further analyzed for the expression of CD206 and MHC class II molecules on the cell surface, as well as for intracellular IL-10 and IL-12 levels. TAMs infiltrating MMTV-PyMT-derived breast carcinomas uniformly expressed IL-10. However, the heterogeneous expression of MHC class II molecules and CD206 demarcated distinct TAM subpopulations (Fig. 1B), consistent with previous reports.<sup>8,26,27</sup> Of note, TAMs failed to express IL-12 (data not shown). Based on these immunological markers, IL-10<sup>+</sup>CD206<sup>+</sup>MHCII<sup>+</sup> macrophages were found to account for more than 80% of TAMs in our system (Fig. 1B and C), an expression profile consistent with a regulatory phenotype<sup>10</sup> and in common with TAMs from mammary carcinomas previously shown to exhibit pro-tumorigenic properties.<sup>2,11</sup>

### The CSF1/CSF1R pathway is required for the turnover of TAMs in mammary tumors

To evaluate the competence of TAMs for signaling via the CSF1/CSF1R pathway, macrophages from spontaneous tumors arising in MMTV-PyMT mice were analyzed for CSF1R expression by flow cytometry. As shown in Figure 1D, CD45<sup>+</sup>CD11b<sup>+</sup>F4/80<sup>+</sup> TAMs stained positively for CSF1R while CD45<sup>-</sup> tumor cells showed no expression of the receptor. We next sought to test the functional dependence of TAMs on signaling mediated by the CSF1/CSF1R pathway. To this end, mice were treated with BLZ945, a small molecule inhibitor of CSF1R kinase activity (Fig. S1), and 5A1, a rat antibody that neutralizes mouse CSF1. Following 6 d of treatment, mammary carcinomas were analyzed by flow cytometry for macrophage (CD45<sup>+</sup>CD11b<sup>+</sup>F4/80<sup>+</sup> cells) and cancer cell (CD45<sup>-</sup> cells) content (Fig. 1E). Treatment with either agent alone significantly reduced the percentage of tumor-infiltrating macrophages (Fig. 1F). No additional decrease in the levels of TAMs were observed in mice treated with both BLZ945 and 5A1 (Fig. 1F), suggesting a functional interdependency between CSF1 and CSF1R in regulating TAMs in this breast cancer model.

In order to determine the kinetics of TAM depletion (and recovery) in response to CSF1R inhibition, we subsequently performed a time-course experiment over a 6–8 d period. We

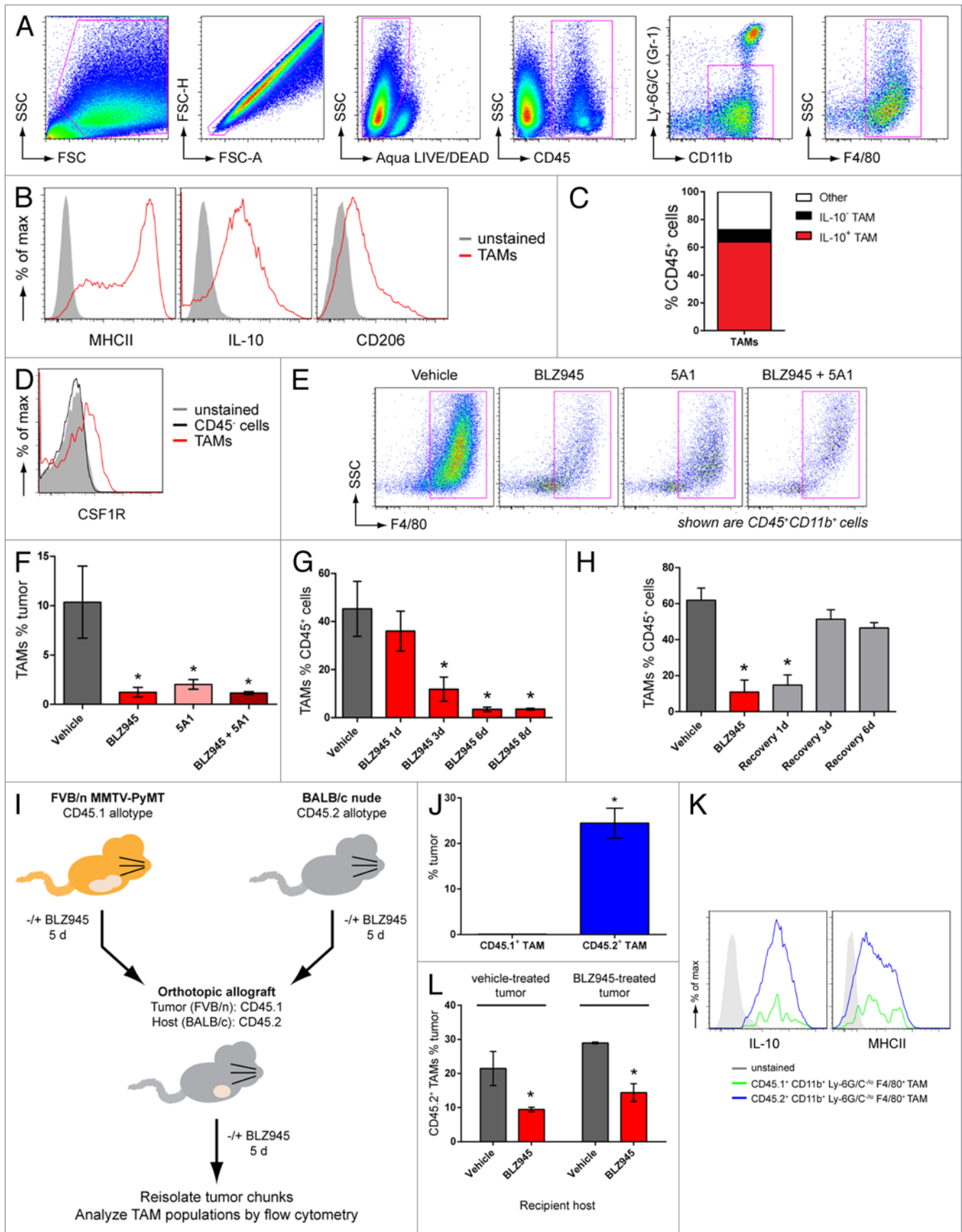


**Figure 1.** See figure legend on following page.

**Figure 1. (See previous page)** The CSF1/CSF1R pathway promotes rapid turnover of regulatory TAMs in MMTV-PyMT mammary tumors. (A–F) Spontaneous mammary tumors in 63 to 77 d old MMTV-PyMT transgenic mice by antibody staining and flow cytometry. (A) Gating strategy to identify CD45<sup>+</sup>CD11b<sup>+</sup>Ly-6G/C(Gr-1)<sup>-lo</sup>F4/80<sup>+</sup> macrophages. Cell populations were gated sequentially from left to right. (B) MHCII, CD206 and intracellular IL-10 expression in CD45<sup>+</sup>CD11b<sup>+</sup>Ly-6G/C(Gr-1)<sup>-lo</sup>F4/80<sup>+</sup> cells (TAMs) identified in (A). Isotype control-stained cells are shown as solid histograms. (C) Mean percentages of IL-10<sup>+</sup> and IL-10<sup>-</sup> TAM subpopulations of total CD45<sup>+</sup> leukocytes isolated from vehicle-treated tumors. (D) Histogram overlay of CSF1R expression in (CD45<sup>+</sup>CD11b<sup>+</sup>Ly-6G/C(Gr-1)<sup>-lo</sup>F4/80<sup>+</sup>) TAMs and CD45<sup>+</sup> tumor cells. Unstained control cells are represented by a solid histogram. (E–F) Flow cytometry data of CD45<sup>+</sup>CD11b<sup>+</sup>F4/80<sup>+</sup> cells (TAMs) from transgenic MMTV-PyMT mice dosed with 200 mg/kg BLZ945, a CSF1R inhibitor, daily or with 5A1, an anti-CSF1 neutralizing antibody (n > 5 per group) at 10 mg/kg every 5 d. TAMs are gated in magenta and values are graphed in (F). (G) Time course of TAM populations in response to 1–8 d of continuous treatment with BLZ945 (n = 4 per group). (H) MMTV-PyMT mice were first dosed with BLZ945 for 5 d (red bar) and then switched to vehicle dosing to provide a recovery period of up to 6 d (gray bars; n = 4 per group). All graphs represent mean values ± SEM \*P < 0.05 vs. vehicle by unpaired t test, 2-tailed. (I–L) Spontaneous tumor pieces from CD45.1<sup>+</sup> FVB/n MMTV-PyMT mice were implanted into a mammary fat pad in CD45.2<sup>+</sup> BALB/C nude mice. Donor and recipient mice were treated with 200 mg/kg BLZ945 or vehicle for 5 d prior to resection and implantation. Five days after implant, tumors were re-isolated and analyzed by flow cytometry. (J) Percentage of tumor-derived CD45.1<sup>+</sup>CD11b<sup>+</sup>Ly-6G/C(Gr-1)<sup>-lo</sup>F4/80<sup>+</sup> TAMs and host-derived CD45.2<sup>+</sup>CD11b<sup>+</sup>Ly-6G/C(Gr-1)<sup>-lo</sup>F4/80<sup>+</sup> TAMs in vehicle-treated tumors implanted into mice dosed with vehicle control. (K) Expression of intracellular IL-10 and cell-surface expression of MHCII in CD45.1<sup>+</sup> (green) and CD45.2<sup>+</sup> (blue) TAM populations. Unstained control cells are shown as solid histograms. (L) Infiltration of CD45.2<sup>+</sup> TAMs into vehicle-treated tumors implanted into mice dosed with vehicle or BLZ945 (n > 11 per group), and BLZ945-treated tumors implanted into mice dosed with vehicle or BLZ945 (n > 7 per group). Bar graphs represent mean values ± SEM. Statistical analyses were performed by 2-tailed unpaired Student t test; \*P < 0.05 vs. vehicle; data shown are representative of at least 2 experiments.

found that TAMs were significantly decreased after as few as 3 d of BLZ945 administration, with maximal inhibition occurring within 6 d of treatment (Fig. 1G). We next sought to evaluate whether, or not, continuous CSF1R inhibition was required to maintain TAM depletion overtime. To address this question, mice were treated with BLZ945 for 6 d and then switched to vehicle during a recovery period of up to 6 d. Complete recovery of TAMs to levels comparable to vehicle-treated mice was observed within 3 d after the removal of BLZ945 (Fig. 1H). Similar kinetics for depletion and recovery were observed for both MHCII<sup>lo</sup> and MHCII<sup>hi</sup> TAM subpopulations (Fig. S2A–E). Considering that the levels of MHCII expression have previously been shown to correlate with distinct differentiation states of TAMs,<sup>8</sup> these findings suggest that the degree of TAM maturation did not alter their sensitivity to BLZ945.

#### The CSF1R pathway promotes the recruitment of TAMs to mammary tumors

Tissue macrophages have a life span ranging from months to years<sup>28</sup> and the relatively rapid kinetics of TAM depletion and recovery observed in our model (Fig. 1G and H) led us to surmise that the CSF1R pathway allows for macrophages to persist within, but also regulates the trafficking of new macrophages to, neoplastic lesions. Specifically, we wondered whether TAMs originates from within the tumor or the surrounding non-malignant mammary gland, and whether the loss of TAMs following CSF1R inhibition was due to impaired recruitment to the neoplasm.

To address this question, we employed a congenic allograft transplantation model comprising 2 mouse strains with distinct CD45 allotypes to discern tumor- and host-derived macrophages. As diagrammed in Figure 1I, spontaneous tumors from FVB/n MMTV-PyMT mice carrying the CD45.1 allotype were orthotopically allografted onto BALB/c nude mice expressing the CD45.2 allotype. Prior to resection and implantation, donor and recipient mice were administered with either BLZ945 (to deplete TAMs) or vehicle (control conditions). Five days after implantation, tumors were re-isolated and analyzed by flow cytometry for the presence of CD45.1<sup>+</sup> tumor-derived and CD45.2<sup>+</sup> host-derived macrophages and determine the relative contributions of these compartments to TAM homeostasis.

In a control setting, in which both donor and recipient mice were treated with vehicle, CD45.1<sup>+</sup> macrophages were barely detectable in the allograft. In sharp contrast, a large CD45.2<sup>+</sup> macrophage population accounted for ~25% of total cells in the tumor (Fig. 1J), a level that is elevated in comparison to that (~10%) typically observed in spontaneous carcinomas in situ (Fig. 1F). Of note, CD45.1<sup>+</sup> and CD45.2<sup>+</sup> TAMs displayed overlapping expression profiles of MHCII and IL-10 (Fig. 1K), indicating that the de novo population of CD45.2<sup>+</sup> macrophages phenotypically resembles CD45.1<sup>+</sup> macrophages originally present in the tumor.

To evaluate the role of CSF1R signaling in the recruitment of macrophages to tumors, donor and/or recipient mice were treated with BLZ945 (Fig. 1I). Vehicle-treated tumors implanted into BLZ945-treated mice contained significantly fewer CD45.2<sup>+</sup> TAMs than those implanted in vehicle-treated mice (Fig. 1L). The levels of CD45.2<sup>+</sup> TAMs were similarly decreased when both tumor and recipient mice were treated with BLZ945 (Fig. 1L). Together, these data indicate that CSF1R inhibition obstructs the recruitment of de novo TAMs from the host. Moreover, mice receiving either vehicle- or BLZ945-treated transplanted tumors showed comparable levels of CD45.2<sup>+</sup> TAM infiltrates (Fig. 1L), suggesting that pre-existent CSF1R-dependent TAMs do not promote additional macrophage infiltration into the tumor.

#### BLZ945-mediated depletion of macrophages is a tissue-specific response

Next, we sought to address whether the reduction in TAMs was due to a systemic decrease in total macrophages or monocyte precursors or a tissue-specific response. Thus, we quantitatively analyzed macrophage content in tumor, liver and lung tissue in 76 to 98 d old female MMTV-PyMT mice by immunohistochemistry using an anti-CSF1R antibody previously reported to label murine macrophages co-expressing CD68 and F4/80.<sup>29</sup> We observed an approximate 6-fold reduction in CSF1R<sup>+</sup> cells within the tumors of BLZ945-treated mice as compared with mice receiving vehicle (Fig. 2A), consistent with the 5-fold reduction in TAMs as measured by flow cytometry. CSF1R<sup>+</sup>-staining Kupffer cells residing in the liver were also reduced 2- to 3-fold in mice treated with

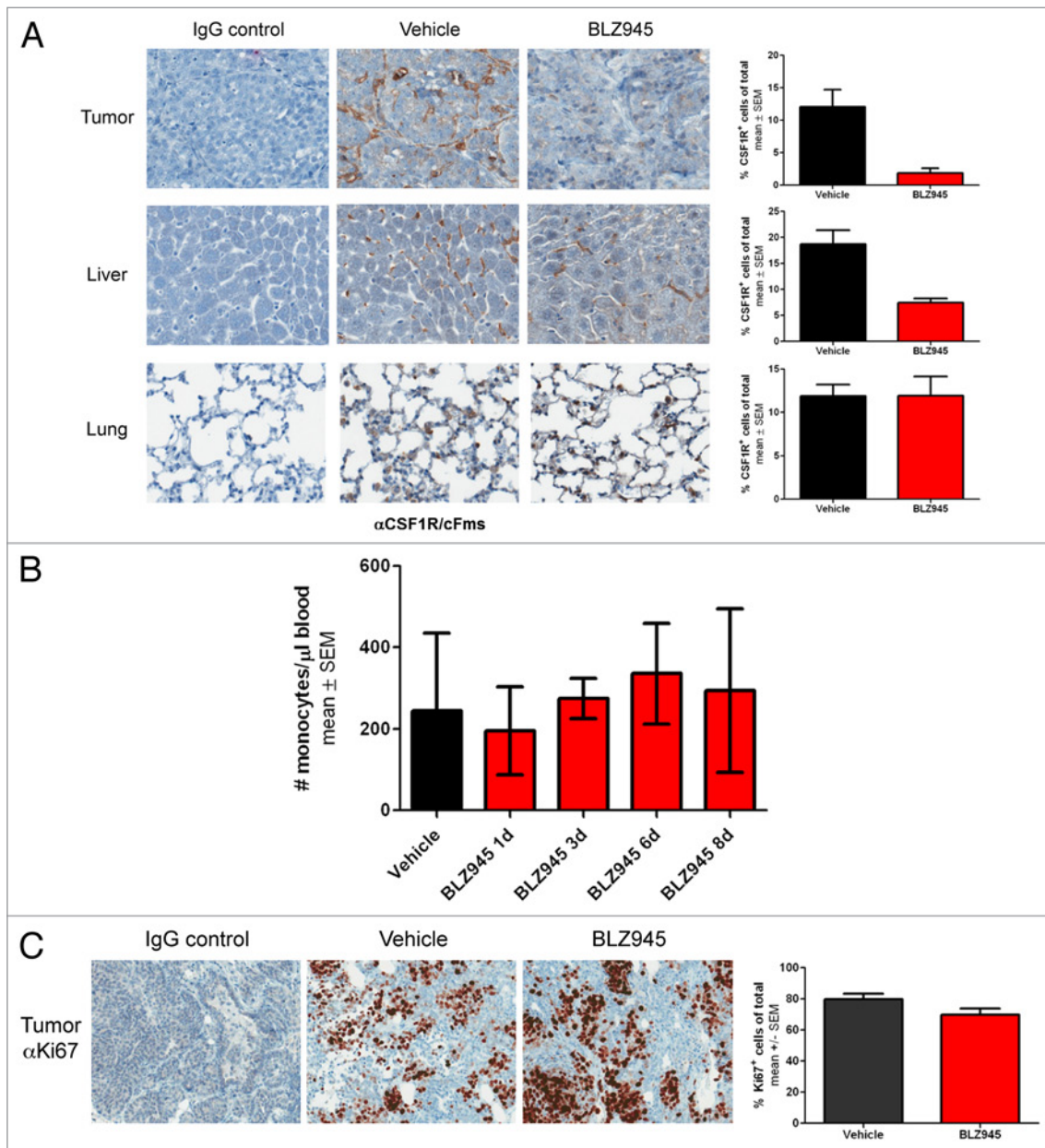


**Figure 2.** Treatment with BLZ945 decreases macrophage content in tumor and liver, but does not affect lung macrophages, circulating monocytes or tumor cell proliferation. (A–C) 56–63 d old female MMTV-PyMT transgenic mice were randomized by tumor volume and dosed with BLZ945 or vehicle control for 16 d ( $n > 3$  per group). Tissues were formalin-fixed and analyzed by immunohistochemistry. Stained slides were scanned using a ScanScope XT and analyzed by ImageScope v11.2 using the positive pixel count algorithm (Aperio Technologies). (A) Tumor, liver and lung sections were stained using an anti-CSF1R antibody to identify macrophages (brown staining). (B) Time course of circulating monocyte numbers in peripheral blood of individual mice ( $n = 4$  per time point). Complete blood counts were performed by IDEXX Laboratories. (C) Tumor tissue was stained using an anti-Ki67 antibody as a measure of proliferation. All graphs represent mean values  $\pm$  SEM.

BLZ945 as compared with control animals. Conversely, the administration of BLZ945 had no effect on the number of CSF1R-expressing macrophages in the lungs (Fig. 2A). In order to determine whether macrophage precursors were depleted by CSF1R inhibition, whole blood from mice treated with BLZ945 or vehicle control was analyzed to determine monocyte counts. As shown in Figure 2B, BLZ945 did not affect the number of circulating monocytes following up to 8 d of continuous treatment.

Previous studies have shown that macrophages and cancer cells engage in a paracrine loop in which macrophages expressing the epidermal growth factor (EGF) promote surrounding neoplastic cells to express CSF1, thereby altering cancer cell proliferation in response to cell-to-cell signals.<sup>30,31</sup> To test whether the reduction in TAMs induced by BLZ945 affected the proliferation of cancer cells, tumor tissue was analyzed by immunohistochemistry using an anti-Ki67 antibody. As shown in Figure 2C, no

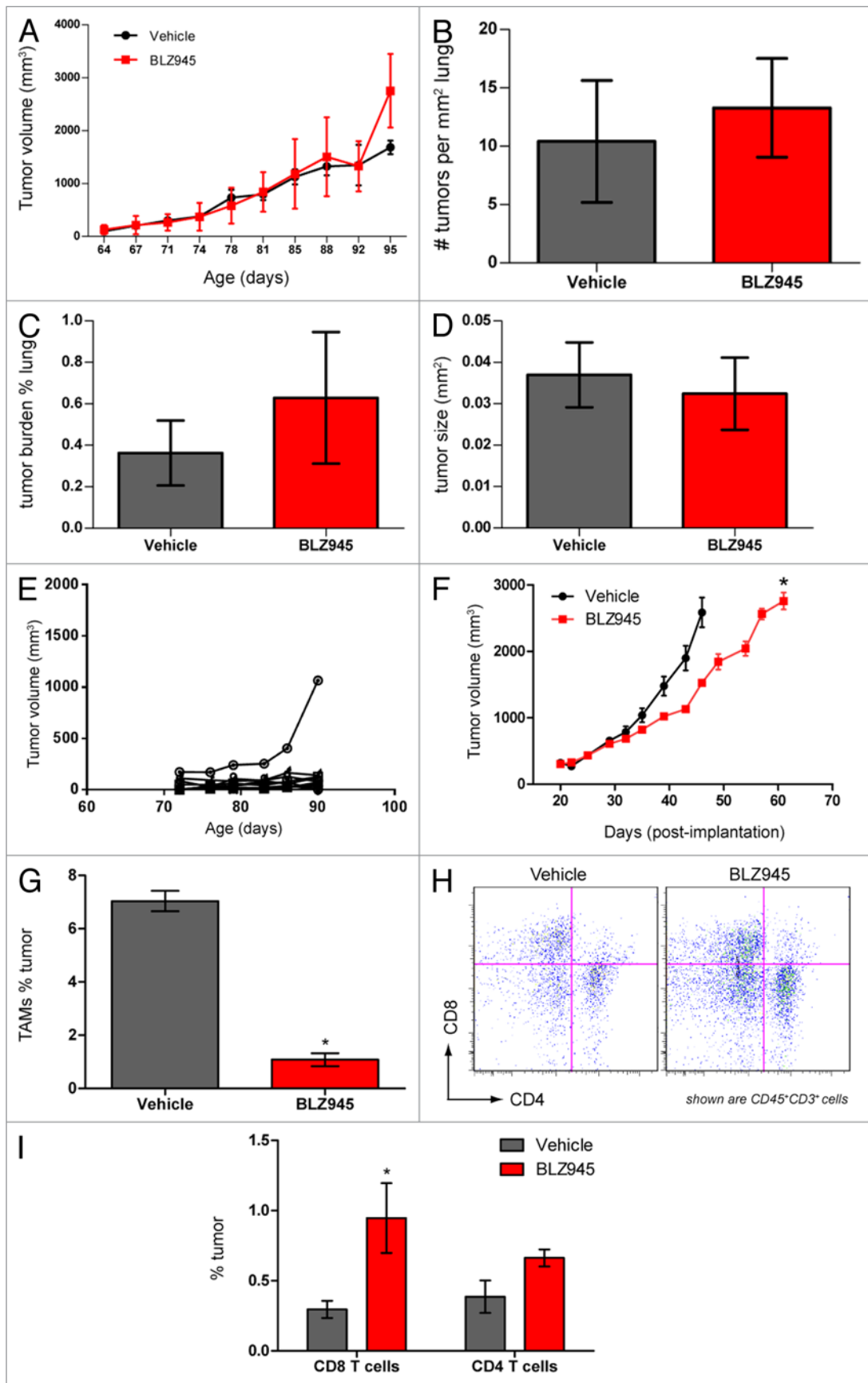


**Figure 3.** See figure legend on following page.

**Figure 3. (See previous page)** Pharmacological blockade of CSF1R signaling increases infiltration of T cells and decreases tumor growth but does not affect pulmonary metastasis in PyMT mice. **(A–E)** 63- to 70-d old MMTV-PyMT transgenic mice were randomized by total tumor burden and dosed with 200 mg/kg BLZ945 or vehicle (n = 9 per group) at the indicated time points. Individual tumor volumes were calculated by caliper measurements with total tumor burden being the sum of these measurements. **(A)** Cumulative tumor burden of vehicle- and BLZ945-dosed mice. **(B)** Lungs from MMTV-PyMT mice were formalin-fixed and serially sectioned to histologically evaluate the number of individual metastases per mm<sup>2</sup> of lung. **(C)** The total metastatic tumor area as a percentage of lung tissue. **(D)** The average area (mm<sup>2</sup>) of lung metastatic spread **(E)** Representative graph showing individual tumor volumes taken from a vehicle-treated mouse. **(F–I)** Spontaneous tumors from naïve MMTV-PyMT mice were pooled and digested to form a single-cell suspension. Cells were injected into mammary fat pads of syngeneic mice. PyMT allograft-recipient mice with average tumor volumes ~280 mm<sup>3</sup> were randomized into 2 groups and dosed with 200 mg/kg BLZ945 or vehicle control 21 d post-implantation. **(F)** Caliper measurements of tumor volumes (n = 6 per group) were taken every 3–4 d. In a separate study, tumors (n = 4 per group) were analyzed by flow cytometry to determine infiltration of **(G)** CD45<sup>+</sup>CD11b<sup>+</sup>Ly-6G/C(Gr-1)<sup>-lo</sup>F4/80<sup>+</sup> TAMs and **(H and I)** CD45<sup>+</sup>CD3<sup>+</sup>CD4<sup>+</sup> and CD45<sup>+</sup>CD3<sup>+</sup>CD8<sup>+</sup> T cells in tumor allografts. Graphs display mean values ± SEM. Statistical analyses were performed by 2-tailed unpaired Student t test; \*P < 0.05 vs. vehicle; data shown are representative of at least 2 experiments.

reduction in Ki67 staining was apparent after 16 d of continuous treatment with BLZ945.

### BLZ945 decreases primary mammary tumor growth but does not affect lung metastatic tumor burden in MMTV-PyMT mice

Consistent with our previous reports using a different CSF1R small molecule inhibitor,<sup>24</sup> we found no significant difference in total tumor burden between 76 to 98 d old vehicle- and BLZ945-treated MMTV-PyMT mice (Fig. 3A). Histopathological analysis of lungs from the same mice carrying cumulative tumor burdens no greater than 2000 mm<sup>3</sup> also showed no difference between vehicle- and BLZ945-treated groups with respect to the density of pulmonary foci (Fig. 3B), cumulative metastatic burden (Fig. 3C), or average size of the foci (Fig. 3D). Due to animal welfare restrictions, we were unable to evaluate tumor growth and metastases in animals bearing late-stage disease. However, in early-stage MMTV-PyMT transgenic mice, we observed a broad variability in the growth kinetics of individual tumors, with the majority of lesions remaining below 300 mm<sup>3</sup> (Fig. 3E). Given the technical challenges of the autochthonous model, we subsequently turned to a more tractable model based on syngeneic orthotopic allografts to monitor tumor growth and the changes in the tumor microenvironment caused by the pharmacological blockade of CSF1 signaling. As in the transgenic model, macrophages accounted for 7–10% of the global cellular content of neoplastic lesions and were reduced in response to BLZ945. Multicolor flow cytometry revealed that the TAMs infiltrating MMTV-PyMT allografts show a similar expression profile of IL-10 and CD206 than the TAMs infiltrating autochthonous tumors (compare Fig. S3 and Figure 1B). Using this model, we found that mice receiving BLZ945 have significantly smaller tumor volumes than their vehicle-treated counterparts (Fig. 3F) and showed a similar fold reduction in TAMs as observed in the autochthonous model (Fig. 3G). This phenotype coincides with a significant increase in CD45<sup>+</sup>CD3<sup>+</sup>CD8<sup>+</sup> T cells in BLZ945-treated tumors as compared with control animals (Fig. 3H and I).

### CSF1R inhibition depletes TAMs, enriches tumor-infiltrating CD8<sup>+</sup> T cells and attenuates the growth of cervical cancer

In order to assess whether the reduction in tumor growth following CSF1R inhibition in the MMTV-PyMT allograft model could also be observed in other settings, we next sought to evaluate the effect of BLZ945 on the K14-HPV-16 transgenic mouse model of cervical carcinogenesis, a model that is also characterized by robust TAM infiltration.<sup>32,33</sup> As diagrammed in Figure 4A,

6 mo old transgenic mice subject to carcinogenic hormonal regimens were continuously treated with BLZ945 (or vehicle control) for 1 mo at the onset of estrogen-dependent cervical cancer. Cervical tumor volumes were determined by histopathological analysis of serial sections, and the mean tumor volume of mice treated with BLZ945 was comparable that of estrogen-naïve T0 control mice, demonstrating tumor stasis (Fig. 4B). Cervical samples were also analyzed by immunohistochemistry using an anti-CSF1R antibody as an indicator of macrophage content (Fig. 4C). Mice receiving BLZ945 showed reduced CSF1R staining in both cervical tumors and the associated stroma, with a significant decrease in CSF1R<sup>+</sup> stromal macrophages relative to vehicle-treated mice (P < 0.05; Figure 4D).

Finally, to determine whether CSF1R inhibition also influenced TAM turnover and T-cell infiltration in cervical carcinoma, 6-mo old tumor-bearing mice were treated with BLZ945 or vehicle for 3–7 d (Fig. 4E). Frozen tissue sections were then analyzed by immunohistochemistry using antibodies against CSF1R, CD4 and CD8 (Fig. 4F–I). Following the administration of BLZ945 for 3 d, mice showed markedly reduced stromal CSF1R staining relative to vehicle-treated mice (Fig. 4F). Consistent with our observations in MMTV-PyMT mice, the administration of BLZ945 (but not that of vehicle) for 5–7 d increased CD8 staining specifically in the tumor-associated stroma (Fig. 4G). In contrast, no difference in CD4 staining was observed between BLZ945- and vehicle-treated mice in either tumor compartment (Fig. 4H).

## Discussion

In this study, we demonstrate that the pharmacological blockade of CSF1R signaling affects both macrophage and T-cell populations associated with mammary and cervical carcinomas. Using the MMTV-PyMT allograft model, we revealed that the inhibition of either CSF1 or CSF1R significantly reduced tumor-infiltrating CD45<sup>+</sup>CD11b<sup>+</sup>Gr-1<sup>-lo</sup>F4/80<sup>+</sup>MHCII<sup>+</sup>IL-10<sup>+</sup>CD206<sup>+</sup> macrophages while increasing the fraction of intratumoral CD45<sup>+</sup>CD3<sup>+</sup>CD8<sup>+</sup> T cells. Furthermore, our results demonstrate that the majority of TAMs in MMTV-PyMT mice display a regulatory phenotype, as defined by expression of IL-10 and CD206. These findings, taken together with the antitumor effects of CSF1R blockade, implicate the CSF1R pathway as a key regulator in the maintenance of an immunosuppressive tumor microenvironment.

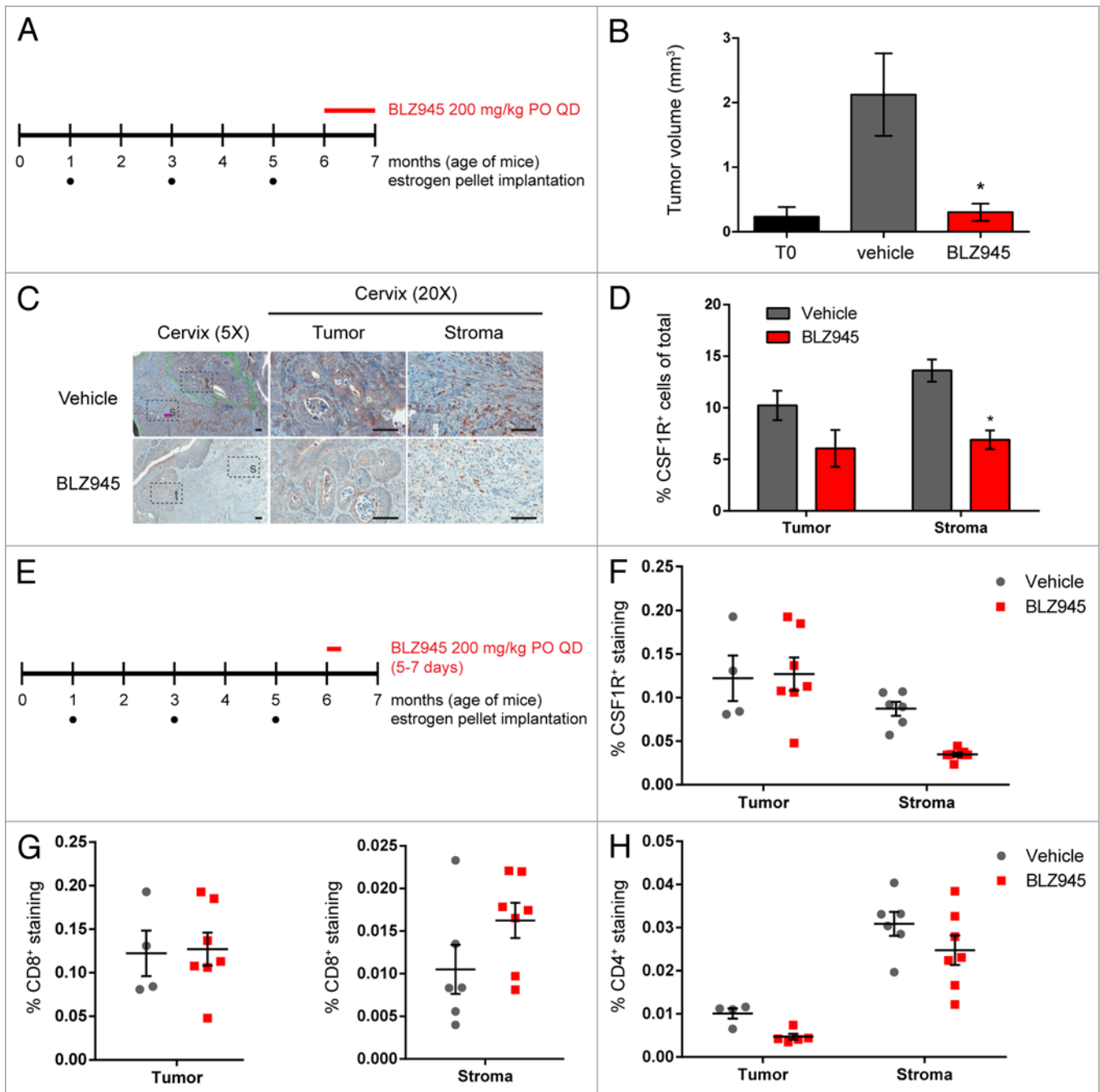


**Figure 4.** Treatment with BLZ945 reduces macrophages, enhances T cell infiltration, and prevents tumor growth in the K14-HPV16 transgenic mouse model of cervical carcinoma. (A–D) Estrogen pellets were administered to 1-mo old K14-HPV16 transgenic mice every 2 mo. Age-matched control mice that did not receive estrogen pellets are referred to as “T0.” At 6 mo of age, mice were dosed with 200 mg/kg BLZ945 or vehicle control for 1 mo, after which time whole cervixes were formalin-fixed for histological analyses. (B) Serial sections of cervical tissue were hematoxylin and eosin (H&E) stained and tumor volumes determined by multiplying the tumor area by the depth of serial sections. Cervical tumors from 6-mo old estrogen-naïve mice (T0) served as a baseline control. (C and D) Cervical tissues were stained with an anti-CSF1R antibody to label macrophages by immunohistochemistry. Magnified views of tumor (t) and stroma (s) regions within the cervix are boxed. Scale bar, 100  $\mu$ m. (D) Quantification of CSF1R staining in cervical tumor and stroma regions. (E–H) Pharmacodynamic study to monitor changes in tumor-infiltrating and stromal immune cells after 5–7 d of treatment with BLZ945. Whole cervixes were frozen, serially sectioned, and stained with H&E to identify the transformation zone. Tumor and stroma regions within the cervix were scored separately for (F) CSF1R<sup>+</sup> macrophages, (G) CD8<sup>+</sup> T cells, and (H) CD4<sup>+</sup> T cells. Bar graphs represent mean values with SEM. Statistical analyses were performed by Mann–Whitney nonparametric test; \* $P < 0.05$  vs. vehicle.

Recent studies have highlighted differential roles for distinct TAM subsets in promoting metastasis in mammary cancer.<sup>12,13,34,35</sup> CCL18-expressing TAMs have been found to promote migration and invasion of breast cancer cells in vitro.<sup>34</sup> Metastasis-associated macrophages have been found to rely on CCL2-CCR2 signaling for metastatic seeding in both the MMTV-PyMT mammary carcinoma model and in a human breast cancer model.<sup>12</sup> TAMs have also been implicated in vessel abnormalization, an effect that is switchable by histidine-rich glycoprotein (HRG).<sup>35</sup> Using a variety of different macrophage markers, we have identified 2 distinct TAM subpopulations characterized by low and high expression of MHCII. Our data are consistent with those of a previous study in which MHCII<sup>hi</sup> and MHCII<sup>lo</sup> TAM populations were identified in TS/A mammary adenocarcinomas, orthotopic 4T1 mammary carcinomas, and subcutaneous 3LL lung carcinomas developing in BALB/c mice,<sup>8</sup> demonstrating that MHCII<sup>hi</sup> and MHCII<sup>lo</sup> TAM subsets are represented in multiple cancer models. We found that MHCII<sup>hi</sup> and MHCII<sup>lo</sup> TAMs were similarly sensitive to BLZ945 and displayed comparable depletion and recovery kinetics. Whether CSF1R signaling regulates all TAMs or only a subset of short-lived TAMs has yet to be determined.

The rapid kinetics of TAM infiltration provides evidence for a continuous signaling between neoplastic lesions and the surrounding tissues. The 3–6 d period of TAM depletion and recovery in BLZ945-treated mice supports a model whereby TAMs are a highly dynamic population constantly undergoing turnover. In a congenic allograft model using donor and recipient mice carrying distinct CD45 allotypes, we found that CD45.2<sup>+</sup> macrophages originating from recipient mice effectively replace the original population of tumor-associated CD45.1<sup>+</sup> macrophages. This rapid turnover occurred within 5 d indicating that TAMs, unlike classical tissue-resident macrophages, persist in tumors for relatively brief periods of time.

Several studies have reported that CSF1 is the major macrophage chemoattractant secreted by tumor cells.<sup>30,36</sup> Given that both macrophages and tumor cells express CSF1,<sup>3</sup> we examined whether TAMs contribute to their own recruitment and found similar levels of CD45.2<sup>+</sup> TAM infiltration in mice receiving vehicle vs. BLZ945 (depleting macrophages) prior to transplantation. This data suggests that TAMs do not appear to be involved in perpetuating their own recruitment, despite expressing CSF1 and other chemokines.

One important consideration is that the BLZ945-mediated inhibition of CSF1R does not fully ablate macrophages in mammary and cervical tumors. From these time-course studies, a residual population of TAMs accounting for less than 1% of the total tumor cells is detectable following 8 d of continuous treatment with BLZ945. This observation is consistent with a study by DeNardo et al., who reported a PLX3397-resistant TAM population that localized to the perivascular space.<sup>24</sup> It is noteworthy that in *Csfl*<sup>op</sup> mice, bearing an inactivating mutation in *Csfl*, macrophage depletion is incomplete and tissue-specific.<sup>23,37</sup> In a transgenic mouse model of proneural glioblastoma multiforme, inhibition of CSF1R by treatment with BLZ945 had no effect on TAM survival but instead inhibited the differentiation of TAMs toward an M2 phenotype, promoting tumor regression.<sup>38</sup>

Altogether, these studies demonstrate that the dependency of different macrophage populations on CSF1/CSF1R varies and is influenced by the local microenvironment.

Multiple approaches have been used to evaluate the role of CSF1/CSF1R signaling in the MMTV-PyMT mammary carcinomas. In a separate study, a dual inhibitor of CSF1R and KIT, PLX3397, was shown to exert no effects on primary tumor growth in MMTV-PyMT allograft-bearing mice, a finding discordant with the decrease in tumor growth that we observed in BLZ945-treated mice.<sup>11</sup> One key distinction between the action of these 2 inhibitors is that the increase in tumor-associated CD8<sup>+</sup> T cells occurring in BLZ945-treated mice is not observed in mice receiving PLX3397 as a single agent. These observations suggest that tumor-infiltrating CD8<sup>+</sup> T cells are potentially critical to the anticancer effects of BLZ945.

Like breast cancer, cervical cancer is characterized by high levels of macrophage infiltration.<sup>39,40</sup> In the HPV-16-driven TC-1 mouse subcutaneous tumor model, M2-like macrophages expressing IL-10 and arginase 1 (ARG1) have been found to constitute the predominant leukocytic infiltrate.<sup>41</sup> The absence of IL-10 function (upon blockade with anti-IL-10 neutralizing antibodies or by injecting TC-1 cells into IL-10-deficient mice) results in delayed tumor growth, increased CD8<sup>+</sup> infiltration and decreased amounts of intratumoral FOXP3<sup>+</sup> regulatory T cells.<sup>42</sup>

To further evaluate the impact of CSF1R signaling in cervical tumorigenesis, we selected the more clinically relevant K14-HPV-16 transgenic model of cervical carcinoma. In comparison to the modest reduction in tumor growth observed in MMTV-PyMT mice treated with BLZ945, we found that the treatment of K14-HPV-16 mice with BLZ945 was sufficient to abrogate cervical tumor growth. Immunohistochemical analyses showed that macrophages were depleted from both neoplastic lesions and the surrounding cervical stroma upon BLZ945 treatment for 30 d. The loss of CSF1R staining in stromal regions within the cervix was also observed in K14-HPV-16 mice treated with BLZ945 for only 5–7 d, a time frame comparable to that needed for BLZ945 to effectively deplete TAMs from MMTV-PyMT mice.

Perhaps the most striking finding of our study was that CD8<sup>+</sup> T cells accumulated within mammary and cervical tumors concurrent with the reduction in macrophages provoked by BLZ945. Consistent with a recent independent study,<sup>24</sup> we observed a preferential increase in CD8<sup>+</sup> T cells compared with CD4<sup>+</sup> T cells upon blockade of CSF1R signaling. The net effect was an increase in the ratio of CD8<sup>+</sup> to CD4<sup>+</sup> T cells, which has been found to be part of a predictive signature for improved disease outcome in breast cancer patients.<sup>11,24</sup> Thus, our findings indicate that CSF1R-dependent TAM activity may aid in tumor immune subversion by actively inhibiting cytotoxic T-cell responses within the tumor microenvironment. Of particular importance, we report that CSF1R signaling maintains a constant and rapid turnover of TAMs in the tumor microenvironment, and that the depletion of TAMs using a highly selective CSF1R inhibitor can arrest or delay the growth of murine cervical and mammary carcinoma, respectively. The single agent efficacy of BLZ945 observed in the cervical cancer model suggests that CSF1R inhibitors, alone or in combination with

chemotherapy, may be especially useful in treating this particular malignancy.

## Materials and Methods

### Genetically engineered mouse models

FVB/N-Tg(MMTV-PyVT)634Mul/J mice were purchased from Jackson Laboratory and bred at Novartis. FVB.Cg-Tg(KRT14-HPV16)wt1Dh mice were obtained from the National Cancer Institute Mouse Repository and bred at Novartis. All mice were maintained under specific pathogen-free conditions at the AAALACI-accredited Novartis Institutes for Biomedical Research vivarium. Housing and experimental animal procedures were approved by the Institutional Animal Care and Use Committee.

### Orthotopic allograft models

6–7 wk old female FVB/NJ mice were purchased from Jackson Laboratory. 6–7 wk old female BALB/c nude mice (CAnN.Cg-Foxn1<sup>nu</sup>/Crl) were obtained from Charles River Laboratory. For the mammary tumor virus-driven Polyoma middle T antigen (MMTV-PyMT) orthotopic allograft model, spontaneous tumors from 10–13 wk old female transgenic MMTV-PyMT mice were pooled and enzymatically digested with Liberase TM (Roche). The resultant single-cell suspension was then immediately injected orthotopically at the indicated cell dosage into a single mammary fat pad of syngeneic female FVB/NJ recipient mice. For the CD45 allotype study, spontaneous tumors from 10–13 wk old female MMTV-PyMT transgenic mice were harvested by blunt dissection and divided into 3 mm cubes. A small incision was made in the mammary fat pad of female BALB/c nude recipient mice and 2 tumor samples were placed inside the fat pad and sealed with surgical staples. After 5 d, the wound was reopened and the tumor samples retrieved. Tumors were digested and analyzed as described below. Donor and recipient mice were treated with either BLZ945 or vehicle for 5 d prior to resection and implantation as described below.

### CSF1-signaling antagonist pharmacological study in spontaneous tumor models

Tumors were measured using calipers and volumes calculated based on the formula: volume = (width)<sup>2</sup> × length/2. In MMTV-PyMT mouse studies, 56–63 d old female mice were randomized into groups based on tumor volumes and dosed with either 20% Captisol® vehicle or 200 mg/kg BLZ945. Dosing was administered by oral gavage once daily and tumor volumes were measured twice weekly. 5A1 rat anti-mouse CSF1 neutralizing antibody or rat IgG control was dosed at 10 mg/kg by intraperitoneal injection every 5 d. To calculate pulmonary metastasis in MMTV-PyMT transgenic mice, formalin-fixed paraffin-embedded lungs were serially sectioned and stained with hematoxylin and eosin (H&E). Tumor regions were scored by tumor burden (total tumor area divided by total lung area), size (tumor diameter), and according to the total number of individual metastases counted in a single-blind fashion. These values were averaged across the entire depth of the lung to obtain the final value. For K14-HPV16 mouse studies, female mice were given slow release 17β-estradiol pellets every 2 mo

to induce squamous carcinogenesis in the cervical and vaginal epithelium.<sup>43,44</sup> Mice were randomized at 6 mo of age at the reported onset of cervical cancer and treated with BLZ945 for a 1 mo duration. To determine cervical tumor volume in K14-HPV16 transgenic mice, formalin-fixed paraffin-embedded cervix tissues and neoplasms were serially sectioned, scored for tumor area in a single-blind fashion, and the values multiplied by the tumor depth.

### Tumor digest

Tumors were harvested by blunt dissection, minced in cold 2% FBS RPMI 1640 and digested with 2.86 Wünsch U/mL Liberase TM (Roche) + 4.29 U/mL DNase I (Roche) for 15 min at room temperature before addition of 0.02% EDTA (EDTA) (Sigma) to stop the digest. Cell suspensions were passed through a 70 μm cell strainer (BD Biosciences) and centrifuged at 4 °C for 5 min at 1500 rpm. After red blood cell (RBC) lysis with 0.86% ammonium chloride, the remaining cells were centrifuged, washed with 2% FBS RPMI 1640 and assayed for viability by Vi-CELL Analyzer (Beckman Coulter).

### Fluorescence cytometry

One–2 million cells were washed with phosphate-buffered saline (PBS) and incubated with rat anti-mouse FCγIII/II receptor (CD16/CD32; clone 93) antibody to block nonspecific binding concurrently with LIVE/DEAD viability stain (Invitrogen) for 15 min at 4 °C. Cells were washed with PBS and incubated with anti-CD3ε (145–2C11), CD4 (GK1.5); CD8a (53–6.7), CD11b (M1/70), CD45 (30-F11), CD45.1 (A20), CD45.2 (104), CD68 (FA-11), CD115/cFMS/CSF1R (AFS98), CD206 (MR5D3), F4/80 (BM8), MHCII (M5/114.15.2; eBioscience), Ly-6G/C(Gr-1) (RB6–8C5) antibodies as indicated. Rat IgG control and Tie-2 (TEK4) antibodies were also used as described. After 30 min, cells were washed with 2% fetal bovine serum (FBS) in PBS + 1 mM EDTA and fixed with BD Stabilizing Fixative (BD Biosciences). Stained cells were stored in 2% FBS in PBS + 1 mM EDTA at 4 °C for up to 72 h. For intracellular staining, cells were permeabilized using BD Perm/Wash (BD Biosciences) and incubated with anti-IL-10 (JES5–16E3), anti-IL-12/23 p40 (C15.6) and anti-IFNγ (XMG1.2) antibodies as indicated. After 30 min., cells were washed in permeabilization buffer followed by 2% FBS in PBS containing 1 mM EDTA. Analysis was performed on 200 000–2 000 000 events collected per sample on an LSRII (BD Biosciences) flow cytometer and analyzed using FlowJo (Tree Star). All antibodies were obtained from BioLegend unless otherwise noted.

### Histology

For paraffin sections, tissues were fixed in 10% buffered formalin for up to 24 h and transferred to 70% ethanol before paraffin embedding. Five 6-μm thick sections were cut using a Leica HM315 microtome. Sections were deparaffinized and rehydrated through an alcohol series prior to histochemical or immunohistochemical staining. Paraffin sections were stained with hematoxylin and eosin (H&E) for histology and anti-cFMS/CD115/CSF1R (1:200, C-20; Santa Cruz) and Ki67 (1:500, SP6; Neomarkers) antibodies for immunohistochemistry. For frozen sections, tissue was embedded without fixation in OCT (Tissue-Tek) and frozen on dry ice. Six-μm thick sections were cut using

a Leica CM1850 cryostat and stored at  $-80^{\circ}\text{C}$ . Frozen sections were air-dried overnight, fixed in ice-cold acetone for 10 min at  $-20^{\circ}\text{C}$ , blocked overnight at  $4^{\circ}\text{C}$  in 5% normal goat serum in PBS with 0.5–2.5% bovine serum albumin (BSA), and incubated for 1 h with anti-cFMS/CD115/CSF1R (1:200, C-20; Santa Cruz), anti-CD4 (1:100, GK1.5; BioLegend), anti-CD8a (1:50, 53–6.7; BioLegend) antibodies or Rabbit IgG control (Ventana Roche), and Rat IgG control (Jackson ImmunoResearch) antibody as indicated. Biotin-conjugated goat anti-rabbit or goat anti-rat IgG (Jackson ImmunoResearch) antibodies were then applied for 32 min in conjunction with the Ventana Discovery Research IHC DAB Map XT kit (Ventana Roche). Stained slides were scanned using a high-resolution digital scanner (ScanScope XT, Aperio Technologies) and analyzed by ImageScope v11.2 using the positive pixel count algorithm (Aperio Technologies).

### Statistics

Data represent mean  $\pm$  SEM of representative experiments. Statistical significance was calculated by student *t* test unless otherwise noted (GraphPad Prism 6), and *P* < 0.05 was considered statistically significant.

### Disclosure of Potential Conflicts of Interest

DCS, at the time of the study, was a Novartis Presidential Postdoctoral Fellow funded by the Novartis Education Office

and the Novartis Institutes for Biomedical Research. Authors YO, NP and DD are employees of the Novartis Institutes for Biomedical Research. The funders had no role in study design and implementation, data analysis, and manuscript preparation. There are no patents, products in development or marketed products involved. The authors declare no conflicting interests.

### Acknowledgments

The authors would like to thank Cyrus Ghajar and Irene Kuhn for helpful discussions, Nicole Vanasse and Brenda Bartholomew for maintaining the transgenic mice, and Sok Chey, Ruben Flores and Jose Lapitan for their support with animal studies. The authors acknowledge support from the Department of Defense Breast Cancer Research Program (BCRP) to B.R., and grants from the NIH/NCI (R01 CA130980, R01CA140943, R01 CA155331, U54 CA163123), the Department of Defense BCRP Era of Hope Scholar Expansion Award (BC10412), the Susan G Komen Foundation (KG11084, KG110560), and the Breast Cancer Research Foundation to LMC.

### Supplemental Materials

Supplemental materials can be found here: <http://www.landesbioscience.com/journals/oncoimmunology/article/26968/>

### References

- Mantovani A, Sica A. Macrophages, innate immunity and cancer: balance, tolerance, and diversity. *Curr Opin Immunol* 2010; 22:231-7; PMID:20144856; <http://dx.doi.org/10.1016/j.coi.2010.01.009>
- Solinas G, Schiara S, Liguori M, Fabbri M, Pesce S, Zammataro L, Pasqualini F, Nebuloni M, Chiabrando C, Mantovani A, et al. Tumor-conditioned macrophages secrete migration-stimulating factor: a new marker for M2-polarization, influencing tumor cell motility. *J Immunol* 2010; 185:642-52; PMID:20530259; <http://dx.doi.org/10.4049/jimmunol.1000413>
- Pollard JW. Trophic macrophages in development and disease. *Nat Rev Immunol* 2009; 9:259-70; PMID:19282852; <http://dx.doi.org/10.1038/nri2528>
- Bingle L, Brown NJ, Lewis CE. The role of tumour-associated macrophages in tumour progression: implications for new anticancer therapies. *J Pathol* 2002; 196:254-65; PMID:11857487; <http://dx.doi.org/10.1002/path.1027>
- Mantovani A, Sozzani S, Locati M, Allavena P, Sica A. Macrophage polarization: tumor-associated macrophages as a paradigm for polarized M2 mononuclear phagocytes. *Trends Immunol* 2002; 23:549-55; PMID:12401408; [http://dx.doi.org/10.1016/S1471-4906\(02\)02302-5](http://dx.doi.org/10.1016/S1471-4906(02)02302-5)
- O'Shea JJ, Murray PJ. Cytokine signaling modules in inflammatory responses. *Immunity* 2008; 28:477-87; PMID:18400190; <http://dx.doi.org/10.1016/j.immuni.2008.03.002>
- Martinez FO, Helming L, Gordon S. Alternative activation of macrophages: an immunologic functional perspective. *Annu Rev Immunol* 2009; 27:451-83; PMID:19105661; <http://dx.doi.org/10.1146/annurev.immunol.021908.132532>
- Movahedi K, Laoui D, Gysemans C, Baeten M, Stangé G, Van den Bossche J, Mack M, Pipeleers D, In't Veld P, De Baetselier P, et al. Different tumor microenvironments contain functionally distinct subsets of macrophages derived from Ly6C(high) monocytes. *Cancer Res* 2010; 70:5728-39; PMID:20570887; <http://dx.doi.org/10.1158/0008-5472.CAN-09-4672>
- Grugan KD, McCabe FL, Kinder M, Greenplate AR, Harman BC, Ekert JE, van Rooijen N, Anderson GM, Nemeth JA, Strohl WR, et al. Tumor-associated macrophages promote invasion while retaining Fc-dependent anti-tumor function. *J Immunol* 2012; 189:5457-66; PMID:23105143; <http://dx.doi.org/10.4049/jimmunol.1201889>
- Mosser DM, Edwards JP. Exploring the full spectrum of macrophage activation. *Nat Rev Immunol* 2008; 8:958-69; PMID:19029990; <http://dx.doi.org/10.1038/nri2448>
- DeNardo DG, Barreto JB, Andreu P, Vasquez L, Tawfik D, Kolhatkar N, Coussens LM. CD4(+) T cells regulate pulmonary metastasis of mammary carcinomas by enhancing protumor properties of macrophages. *Cancer Cell* 2009; 16:91-102; PMID:19647220; <http://dx.doi.org/10.1016/j.ccr.2009.06.018>
- Qian BZ, Li J, Zhang H, Kitamura T, Zhang J, Campion LR, Kaiser EA, Snyder LA, Pollard JW. CCL2 recruits inflammatory monocytes to facilitate breast-tumour metastasis. *Nature* 2011; 475:222-5; PMID:21654748; <http://dx.doi.org/10.1038/nature10138>
- Qian B, Deng Y, Im JH, Muschel RJ, Zou Y, Li J, Lang RA, Pollard JW. A distinct macrophage population mediates metastatic breast cancer cell extravasation, establishment and growth. *PLoS One* 2009; 4:e6562; PMID:19668347; <http://dx.doi.org/10.1371/journal.pone.0006562>
- Qian BZ, Pollard JW. Macrophage diversity enhances tumor progression and metastasis. *Cell* 2010; 141:39-51; PMID:20371344; <http://dx.doi.org/10.1016/j.cell.2010.03.014>
- Tang R, Beuvon F, Ojeda M, Mosseri V, Pouillart P, Scholl S. M-CSF (monocyte colony stimulating factor) and M-CSF receptor expression by breast tumour cells: M-CSF mediated recruitment of tumour infiltrating monocytes? *J Cell Biochem* 1992; 50:350-6; PMID:1334964; <http://dx.doi.org/10.1002/jcb.240500403>
- Cohen PE, Chisholm O, Arceci RJ, Stanley ER, Pollard JW. Absence of colony-stimulating factor-1 in osteopetrotic (csfmop/csfmop) mice results in male fertility defects. *Biol Reprod* 1996; 55:310-7; PMID:8828834; <http://dx.doi.org/10.1095/biolreprod55.2.310>
- Dai XM, Ryan GR, Hapel AJ, Dominguez MG, Russell RG, Kapp S, Sylvestre V, Stanley ER. Targeted disruption of the mouse colony-stimulating factor 1 receptor gene results in osteopetrosis, mononuclear phagocyte deficiency, increased primitive progenitor cell frequencies, and reproductive defects. *Blood* 2002; 99:111-20; PMID:11756160; <http://dx.doi.org/10.1182/blood.V99.1.111>
- Lin H, Lee E, Hestir K, Leo C, Huang M, Bosch E, Halenbeck R, Wu G, Zhou A, Behrens D, et al. Discovery of a cytokine and its receptor by functional screening of the extracellular proteome. *Science* 2008; 320:807-11; PMID:18467591; <http://dx.doi.org/10.1126/science.1154370>
- Wei S, Nandi S, Chitu V, Yeung YG, Yu W, Huang M, Williams LT, Lin H, Stanley ER. Functional overlap but differential expression of CSF-1 and IL-34 in their CSF-1 receptor-mediated regulation of myeloid cells. *J Leukoc Biol* 2010; 88:495-505; PMID:20504948; <http://dx.doi.org/10.1189/jlb.1209822>
- Lin EY, Gouon-Evans V, Nguyen AV, Pollard JW. The macrophage growth factor CSF-1 in mammary gland development and tumor progression. *J Mammary Gland Biol Neoplasia* 2002; 7:147-62; PMID:12465600; <http://dx.doi.org/10.1023/A:1020399802795>

21. Sharma M, Beck AH, Webster JA, Espinosa I, Montgomery K, Varma S, van de Rijn M, Jensen KC, West RB. Analysis of stromal signatures in the tumor microenvironment of ductal carcinoma in situ. *Breast Cancer Res Treat* 2010; 123:397-404; PMID:19949854; <http://dx.doi.org/10.1007/s10549-009-0654-0>
22. Beck AH, Espinosa I, Edris B, Li R, Montgomery K, Zhu S, Varma S, Marinelli RJ, van de Rijn M, West RB. The macrophage colony-stimulating factor 1 response signature in breast carcinoma. *Clin Cancer Res* 2009; 15:778-87; PMID:19188147; <http://dx.doi.org/10.1158/1078-0432.CCR-08-1283>
23. Lin EY, Nguyen AV, Russell RG, Pollard JW. Colony-stimulating factor 1 promotes progression of mammary tumors to malignancy. *J Exp Med* 2001; 193:727-40; PMID:11257139; <http://dx.doi.org/10.1084/jem.193.6.727>
24. DeNardo DG, Brennan DJ, Rexhepaj E, Ruffell B, Shiao SL, Madden SF, Gallagher WM, Wadhvani N, Keil SD, Junaid SA, et al. Leukocyte complexity predicts breast cancer survival and functionally regulates response to chemotherapy. *Cancer Discov* 2011; 1:54-67; PMID:22039576; <http://dx.doi.org/10.1158/2159-8274.CD-10-0028>
25. Coussens LM, Hanahan D, Arbeit JM. Genetic predisposition and parameters of malignant progression in K14-HPV16 transgenic mice. *Am J Pathol* 1996; 149:1899-917; PMID:8952526
26. Mazzei R, Pucci F, Moi D, Zonari E, Ranghetti A, Berti A, Politi LS, Gentner B, Brown JL, Naldini L, et al. Targeting the ANG2/TIE2 axis inhibits tumor growth and metastasis by impairing angiogenesis and disabling rebounds of proangiogenic myeloid cells. *Cancer Cell* 2011; 19:512-26; PMID:21481792; <http://dx.doi.org/10.1016/j.ccr.2011.02.005>
27. Pucci F, Venneri MA, Bizziato D, Nonis A, Moi D, Sica A, Di Serio C, Naldini L, De Palma M. A distinguishing gene signature shared by tumor-infiltrating Tie2-expressing monocytes, blood "resident" monocytes, and embryonic macrophages suggests common functions and developmental relationships. *Blood* 2009; 114:901-14; PMID:19383967; <http://dx.doi.org/10.1182/blood-2009-01-200931>
28. van Furth R, Cohn ZA, van FR. The origin and kinetics of mononuclear phagocytes. *J Exp Med* 1968; 128:415-35; PMID:5666958; <http://dx.doi.org/10.1084/jem.128.3.415>
29. Ruffell B, Au A, Rugo HS, Esserman LJ, Hwang ES, Coussens LM. Leukocyte composition of human breast cancer. *Proc Natl Acad Sci U S A* 2012; 109:2796-801; PMID:21825174; <http://dx.doi.org/10.1073/pnas.1104303108>
30. Goswami S, Sahai E, Wyckoff JB, Cammer M, Cox D, Pixley FJ, Stanley ER, Segall JE, Condeelis JS. Macrophages promote the invasion of breast carcinoma cells via a colony-stimulating factor-1/epidermal growth factor paracrine loop. *Cancer Res* 2005; 65:5278-83; PMID:15958574; <http://dx.doi.org/10.1158/0008-5472.CAN-04-1853>
31. Patsialou A, Wyckoff J, Wang Y, Goswami S, Stanley ER, Condeelis JS. Invasion of human breast cancer cells in vivo requires both paracrine and autocrine loops involving the colony-stimulating factor-1 receptor. *Cancer Res* 2009; 69:9498-506; PMID:19934330; <http://dx.doi.org/10.1158/0008-5472.CAN-09-1868>
32. Giraudo E, Inoue M, Hanahan D. An amino-bisphosphonate targets MMP-9-expressing macrophages and angiogenesis to impair cervical carcinogenesis. *J Clin Invest* 2004; 114:623-33; PMID:15343380
33. Daniel D, Chiu C, Giraudo E, Inoue M, Mizzen LA, Chu NR, Hanahan D. CD4+ T cell-mediated antigen-specific immunotherapy in a mouse model of cervical cancer. *Cancer Res* 2005; 65:2018-25; PMID:15753402; <http://dx.doi.org/10.1158/0008-5472.CAN-04-3444>
34. Chen J, Yao Y, Gong C, Yu F, Su S, Chen J, Liu B, Deng H, Wang F, Lin L, et al. CCL18 from tumor-associated macrophages promotes breast cancer metastasis via PITPNM3. *Cancer Cell* 2011; 19:541-55; PMID:21481794; <http://dx.doi.org/10.1016/j.ccr.2011.02.006>
35. Rolny C, Mazzone M, Tugues S, Laoui D, Johansson I, Coulon C, Squadrito ML, Segura I, Li X, Knevels E, et al. HRG inhibits tumor growth and metastasis by inducing macrophage polarization and vessel normalization through downregulation of PlGF. *Cancer Cell* 2011; 19:31-44; PMID:21215706; <http://dx.doi.org/10.1016/j.ccr.2010.11.009>
36. Wyckoff J, Wang W, Lin EY, Wang Y, Pixley F, Stanley ER, Graf T, Pollard JW, Segall J, Condeelis J. A paracrine loop between tumor cells and macrophages is required for tumor cell migration in mammary tumors. *Cancer Res* 2004; 64:7022-9; PMID:15466195; <http://dx.doi.org/10.1158/0008-5472.CAN-04-1449>
37. Witmer-Pack MD, Hughes DA, Schuler G, Lawson L, McWilliam A, Inaba K, Steinman RM, Gordon S. Identification of macrophages and dendritic cells in the osteopetrotic (op/op) mouse. *J Cell Sci* 1993; 104:1021-9; PMID:8314887
38. Pyonteck SM, Akkari L, Schuhmacher AJ, Bowman RL, Sevenich L, Quail DF, Olson OC, Quick ML, Huse JT, Teijeiro V, et al. CSF-1R inhibition alters macrophage polarization and blocks glioma progression. *Nat Med* 2013; 19:1264-72; PMID:24056773; <http://dx.doi.org/10.1038/nm.3337>
39. Hammes LS, Tekmal RR, Naud P, Edelweiss MI, Kirma N, Valente PT, Syrjänen KJ, Cunha-Filho JS. Macrophages, inflammation and risk of cervical intraepithelial neoplasia (CIN) progression-clinicopathological correlation. *Gynecol Oncol* 2007; 105:157-65; PMID:17229459; <http://dx.doi.org/10.1016/j.ygyno.2006.11.023>
40. Mazibrada J, Rittà M, Mondini M, De Andrea M, Azzimonti B, Borgogna C, Ciotti M, Orlando A, Surico N, Chiusa L, et al. Interaction between inflammation and angiogenesis during different stages of cervical carcinogenesis. *Gynecol Oncol* 2008; 108:112-20; PMID:17936343; <http://dx.doi.org/10.1016/j.ygyno.2007.08.095>
41. Lepique AP, Daghasanli KR, Cuccovia IM, Villa LL. HPV16 tumor associated macrophages suppress antitumor T cell responses. *Clin Cancer Res* 2009; 15:4391-400; PMID:19549768; <http://dx.doi.org/10.1158/1078-0432.CCR-09-0489>
42. Bolpetti A, Silva JS, Villa LL, Lepique AP. Interleukin-10 production by tumor infiltrating macrophages plays a role in Human Papillomavirus 16 tumor growth. *BMC Immunol* 2010; 11:27; PMID:20525400; <http://dx.doi.org/10.1186/1471-2172-11-27>
43. Arbeit JM, Howley PM, Hanahan D. Chronic estrogen-induced cervical and vaginal squamous carcinogenesis in human papillomavirus type 16 transgenic mice. *Proc Natl Acad Sci U S A* 1996; 93:2930-5; PMID:8610145; <http://dx.doi.org/10.1073/pnas.93.7.2930>
44. Elson DA, Riley RR, Lacey A, Thordarson G, Talamantes FJ, Arbeit JM. Sensitivity of the cervical transformation zone to estrogen-induced squamous carcinogenesis. *Cancer Res* 2000; 60:1267-75; PMID:10728686